REPORT DOCUMENTATION PAGE

Form Approved
OMB No. 0704-0188

1. REPORT DATE *(DD-MM-YYYY)*	**2. REPORT TYPE**	**3. DATES COVERED** *(From - To)*
22-12-2016	Final Report	7/1/15 to 12/22/16

4. TITLE AND SUBTITLE
Deep Water Ocean Acoustics

5a. CONTRACT NUMBER
N00014-14-C-0172

5b. GRANT NUMBER

5c. PROGRAM ELEMENT NUMBER

6. AUTHOR(S)
Dr. Kevin Heaney

5d. PROJECT NUMBER

5e. TASK NUMBER

5f. WORK UNIT NUMBER

7. PERFORMING ORGANIZATION NAME(S) AND ADDRESS(ES)

Ocean Acoustical Services and
Instrumentation Systems, Inc.
5 Militia Drive, Ste. 104
Lexington, MA 02421-4706

8. PERFORMING ORGANIZATION REPORT NUMBER
FR-14C0172-Ocean Acoustics-123116

9. SPONSORING / MONITORING AGENCY NAME(S) AND ADDRESS(ES)
Office of Naval Research
ONR 253
875 North Randolph Street
Arlington, VA 22203-1995

10. SPONSOR/MONITOR'S ACRONYM(S)
ONR

11. SPONSOR/MONITOR'S REPORT NUMBER(S)
Final Report

12. DISTRIBUTION / AVAILABILITY STATEMENT
Distribution Statement A. Approved for public release; distribution is unlimited

13. SUPPLEMENTARY NOTES

14. ABSTRACT In this work for code 32 (Ocean Acoustics) of the Office of Naval Research, OASIS has focused on the development of new propagation models and their application to problems in acoustic propagation in deep water, including global scale acoustic propagation relevant to geophysics sound sources (volcanoes/earthquakes) and the detection of nuclear test event. The Peregrine PE model was developed as an re-coding in C of the Range-dependent Acoustic Model (RAM). This code was extended to 3-dimensions by applying the split-step Pade kernel in cross-range at each range step. The kernel of Peregrine (Seahawks) has been submitted to the Ocean Atmospheric Media Library (OAML). Peregrine was applied to hydroacoustic recordings from a Comprehensive Test Ban Treaty Organization (CTBTO) of a seismic tomography experiment off of Japan, with excellent quantitative agreement in both the energy received and the travel time, both exhibiting strong 3D propagation. A paper was published on using noise correlations to estimate local sound speed, as well as the horizontal deflection caused by mesoscale eddies as they traverse long ranges. Propagation and ambient noise analysis was conducted on the North Pacific Acoustics Laboratory Philippine Sea tests 2009 and 2010, both of which Dr. Heaney participated as a co-chief scientist.

15. SUBJECT TERMS
Global hydroacoustics, three-dimensional propagation, parabolic equation modeling, deep ocean ambient noise

16. SECURITY CLASSIFICATION OF:			**17. LIMITATION OF ABSTRACT**	**18. NUMBER OF PAGES**	**19a. NAME OF RESPONSIBLE PERSON**
a. REPORT	**b. ABSTRACT**	**c. THIS PAGE**			Kevin Heaney
U	U	U	UU	27	**19b. TELEPHONE NUMBER** *(include area code)* 703-346-3676

Final Report

Technical and Financial

Deep Water Ocean Acoustics
Award No.: N00014-14-C-0172

Report No. FR-14C0172-Ocean Acoustics-123116
Prepared for: Office of Naval Research
For the period: July 1, 2015 to December 30, 2016

Submitted by:
Principal Investigator/Author: Kevin Heaney
Ocean Acoustical Services and Instrumentation Systems, Inc.
5 Militia Drive
Lexington, MA 02421

Date Submitted: December 22, 2016

Notices:

Contents

Technical Final Report

1. Introduction

The goal of this research is to increase our understanding of the impact of the ocean and seafloor environmental variability on deep-water (long-range) ocean acoustic propagation and to develop methodologies for including this in acoustic models. Experimental analysis is combined with model development to isolate specific physics and improve our understanding. During the past few years, the physics effects studied have been three-dimensional propagation on global scales, deep water ambient noise, under-ice scattering, bathymetric diffraction and the application of the ocean acoustic Parabolic Equation to infrasound.

2. Peregrine Development

The Parabolic Equation model Peregrine was developed under the Office of Naval Research Ocean Acoustics Code 32 funding. In order to benchmark Peregrine against both RAM and NSPE, work was conducted to set up and run specific range-dependent benchmark problems. During this period of performance Dr. Heaney successfully completed the comparison of Peregrine to RAM for range-independent and range-dependent cases. This was done at 250 Hz, 1kHz and 3.5 kHz. In order to get the models to agree the following things had to be done:

1.) Adjusted the Peregrine water depth so that the seafloor depth matched that of RAM (this involved 1 grid shortening of the water column);
2.) Explicitly defined the geo-acoustics so that both models had the same sponge;
3.) Output the complete computational grid, and smoothed both results after the fact, rather than using the code discrete output; and
4.) Turned off Thorp attenuation.

A single example of this comparison is shown in Figure 1 below, where for a range-dependent environment (flat, upslope, flat) RAM is compared with Peregrine.

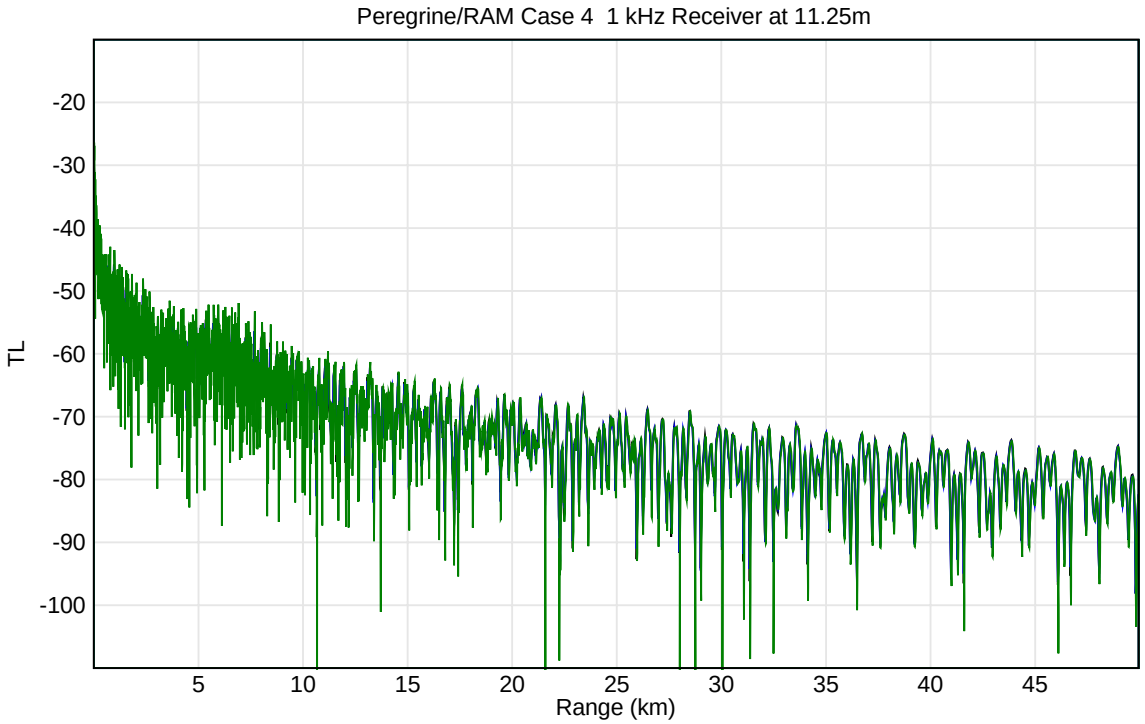

Figure 1. Range-dependent (upslope) comparison of Peregrine and RAM for 1 kHz.

The kernel of Peregrine is a small subroutine named Seahawk. Seahawk.c, as a subroutine, can be directly integrated into NSPE (Navy Standard Parabolic Equation), permitting testing of the Seahawk/Peregrine algorithm without worrying about environmental interpretation. This procedure was performed and documented. The NSPE and NSPE_Seahawk comparison for the NSPE test case 5 is shown below. Agreement is excellent.

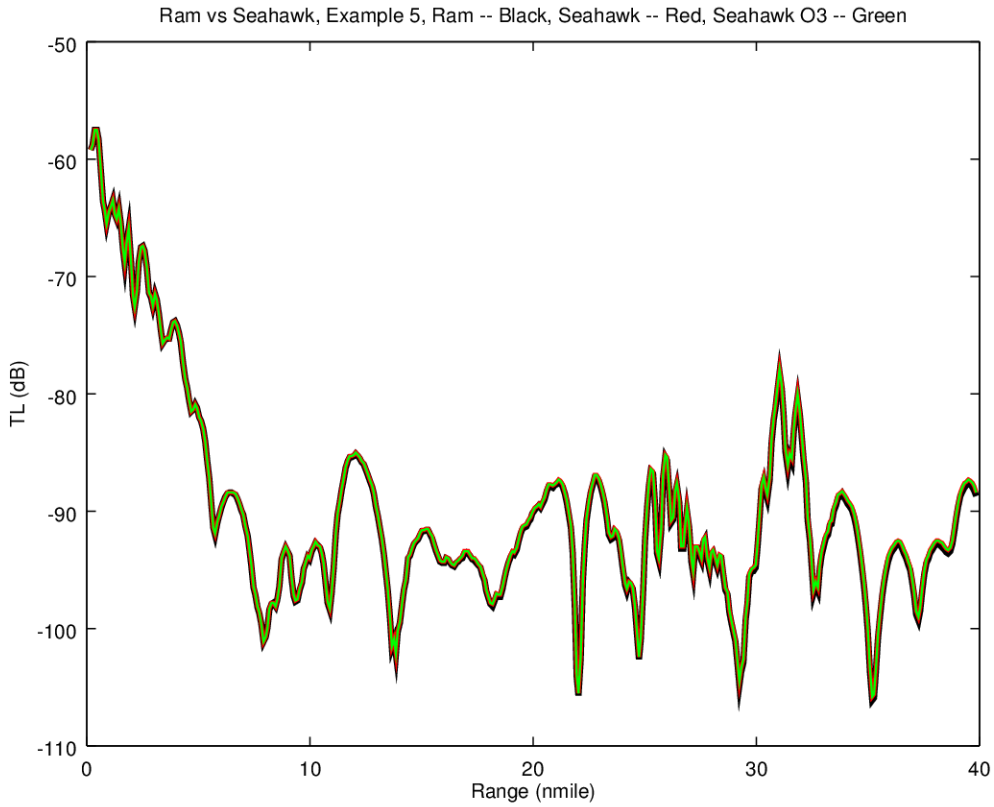

Figure 2. Range-dependent (Downslope) comparison of NSPE and NSPE w/ RAM for the NSPE Test Case 5.

3. Basin Scale Acoustics and CTBTO Data Analysis

3.1. Basin Scale Acoustic Propagation and CTBTO Data Analysis

The paper "*Three-dimensional parabolic equation modeling of mesoscale eddy deflection*", by Heaney and Campbell, was published in JASA in February of 2016. This paper introduces the Peregrine model to the community and establishes its capability for performing global scale 3D propagation experiments. Dr. Heaney also completed and submitted the paper "*Bathymetric diffraction of basin-scale hydroacoustic signals*", by Heaney, Campbell and Mark Prior (TNO/CTBTO) describing observations and modeling of seismic events in the acoustic shadow of large land masses (South Georgia Island and South America).

Work was conducted evaluating the arrivals of a series of explosive shots dropped by Japanese Seismologists off the coast of Japan. Explosions from these two tests, (Normal Mantle – NOMAN) and JT (Japanese Trough) were both detected 19000 km

away at the Juan Fernandez (HA03) station of the International Monitoring System of the Comprehensive Test Ban Treaty Organization.

The first set of runs were from HA03 over the entire globe, at a frequency of 4Hz, for both 2-dimensional and 3-dimensional propagation. The 3D propagation result is shown in Figure 3.

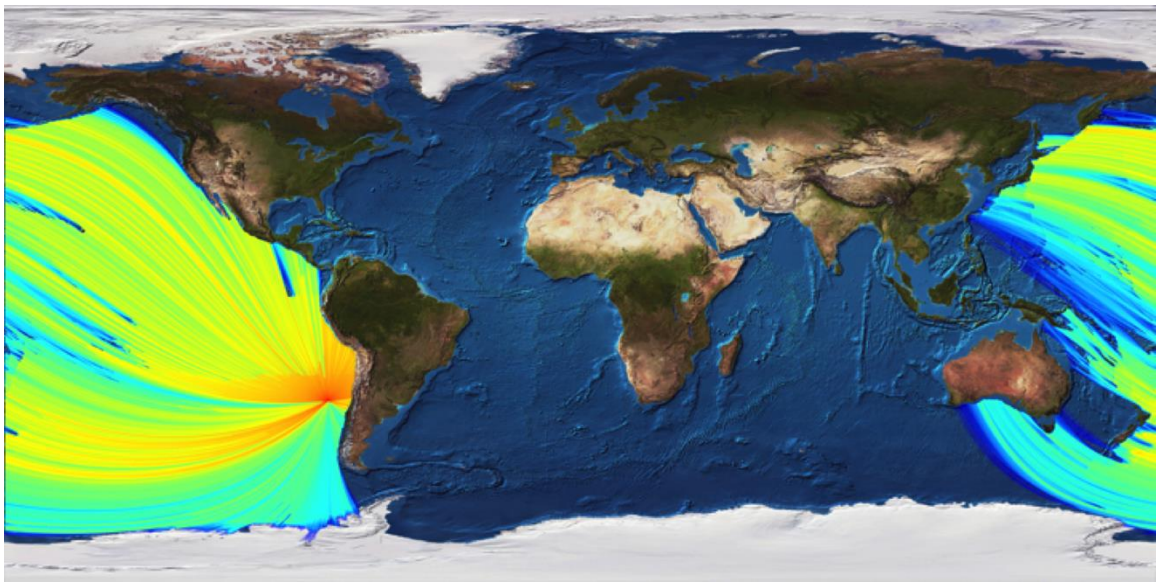

Figure 3. 4Hz Transmission Loss using 3D Peregrine Model for HA03N (Juan Fernandez) CTBTO Receiver

Of interest to these measurements from sources off Japan is the blockage of the Hawaiian Archipelago. There is also a row of seamounts off the coast of northern Chile, which scatter and diffract sound. Dr. Tomoaki Yamada, of the University of Tokyo, has spent the past year at CTBTO in Vienna processing the data from both tests. Of interest to us is the levels of arrivals from the Japan Trough site, which should be in the shadow of the Hawaiian Islands. Work is also being done to calibrate the source spectra, which for a large explosion is much more complicated than the impulse response typically modeled using the PE. Bubble pulse effects will significantly increase the pulse duration even without propagation effects. The final research topic is the multiple arrivals at HA11 (Wake Island). These will be explored in future work.

Comparing the receiver power from each pulse (in a band-passed 4-20Hz window over 20s) with the 2D incoherent (4-20Hz) shows significant discrepancies (Figure 4). In particular, for the Northern portion where the two legs intersect, there is substantial energy. For the 2D computation, there is no received energy as this point is in the shadow behind the big Island of Hawaii. Note that care has not been applied to calibrate the two figures.

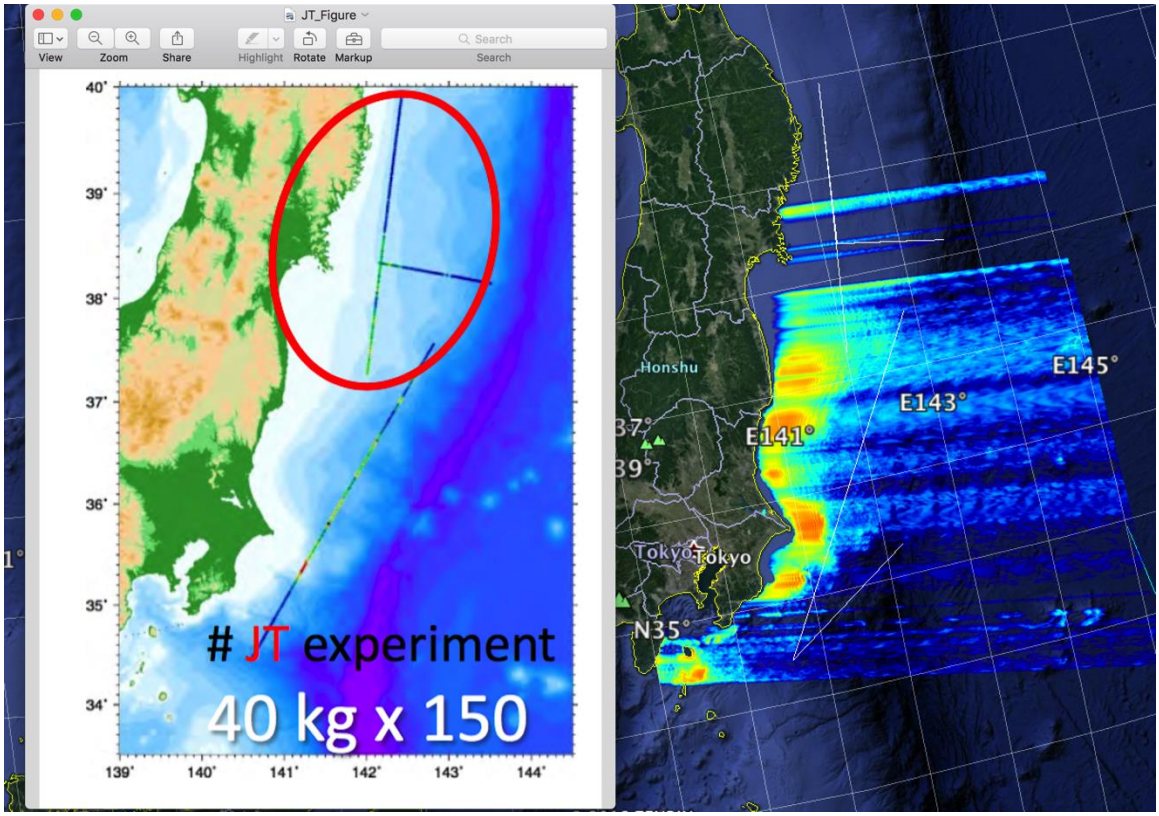

Figure 4. Observed total power (left) compared with the 2D PE modeled total incoherent power (right) for the Japan Trough Experiment. Note the lack of energy in the model at the T-junction east of Japan at 39°N latitude.

The same model computation was performed with the 3D propagation kernel (split-step Pade with 4 Pade terms). These results are shown in Figure 5.

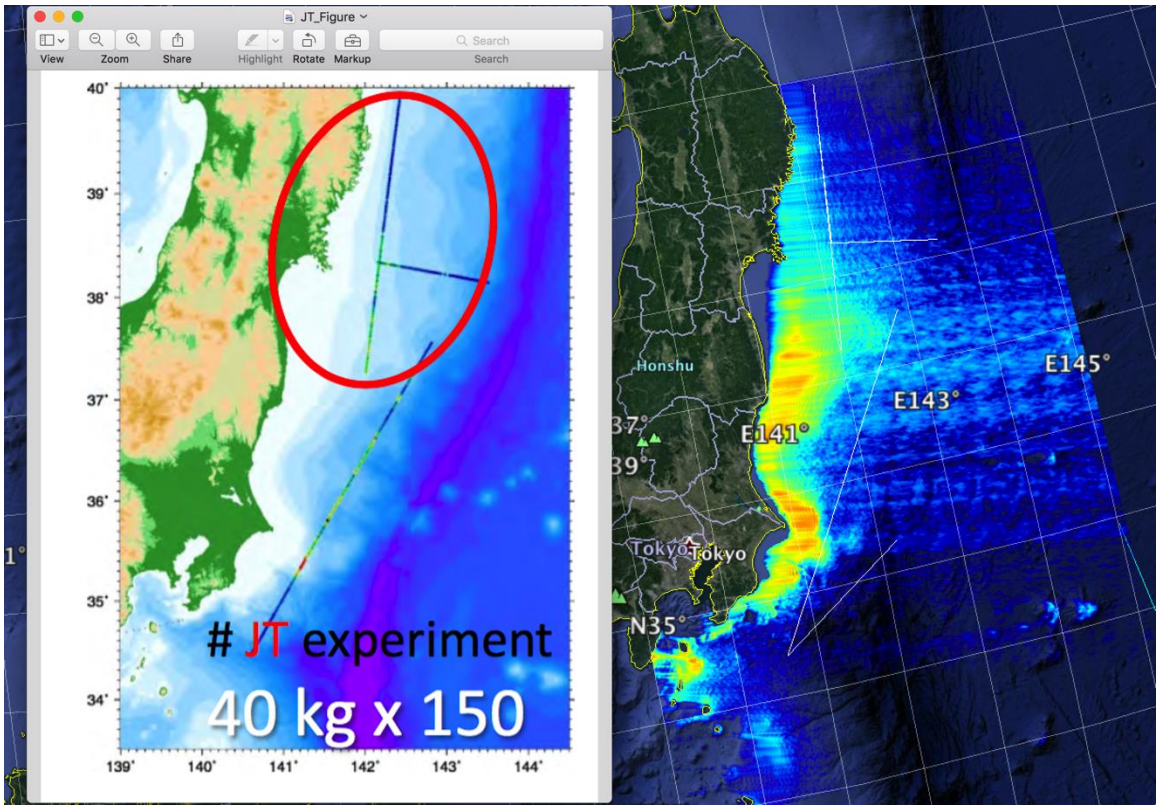

Figure 5. Observed total power (left) compared with the 3D PE modeled total incoherent power (right) for the Japan Trough Experiment. Note the lack of energy in the model at the T-junction east of Japan at 39°N latitude.

The 3D model includes diffraction from the Hawaiian Islands, and from the ridge north of the HA03 receiver stations. The resulting field from the Japan coast shows no distinct shadows, entirely consistent with the observations of Yamada. The fall off of received level as the transects move north, as well as east into deeper water is also modeled well.

The Parabolic Equation Model Peregrine, was applied to observations made at the United Nations Comprehensive Test Ban Treaty Organization (CTBTO) of a set of 100 shots deployed off of the coast of Japan. These measurements were made by Prof. Tomoaki Yamada, from the University of Tokyo. This work is also in collaboration with Dr. Mario Zampolli and Dr. Georgios Haralabus of the CTBTO. These were recorded over 190000 km away at the Juan Fernandez receiver site (HA03). The 3D PE was run, using reciprocity, from Juan Fernandez, Chile to each shot location off the coast of Japan. Peregrine has an option where the 3D code can be computed along a tube centered on the geodesic path. Initially this computational tube was set to 300km, as it was expected that the energy received in the shadow of Hawaii would refract around small islands and fill in the shadow. This turned out not to be the case. The energy observed in the shadow of the Hawaiian Islands is refracted from Midway, and thus the width of the computational tube must be set to 1000 km. The 2D / 3D global run, incoherently averaged (in Intensity) from 4 to 20 Hz for a receiver depth of 30-90m is shown in Figure 6. The

persistence of shadows in the 2D plot (upper panel) is the primary difference. There are 3 places where significant bathymetric interaction occurs and 3D diffraction dominates. The first is the South East Pacific Rise, just northwest of Juan Fernandez at a Latitude of roughly 28°S. The second is the Hawaiian Island Chain, extending to Midway Island at 28°N, 177°W and finally the Emperor Seamount chain running due north at 170°E. The effect of these bathymetric interactions is to fill the shadow zone completely by the time the Asian continent is encountered at the Japan coastline.

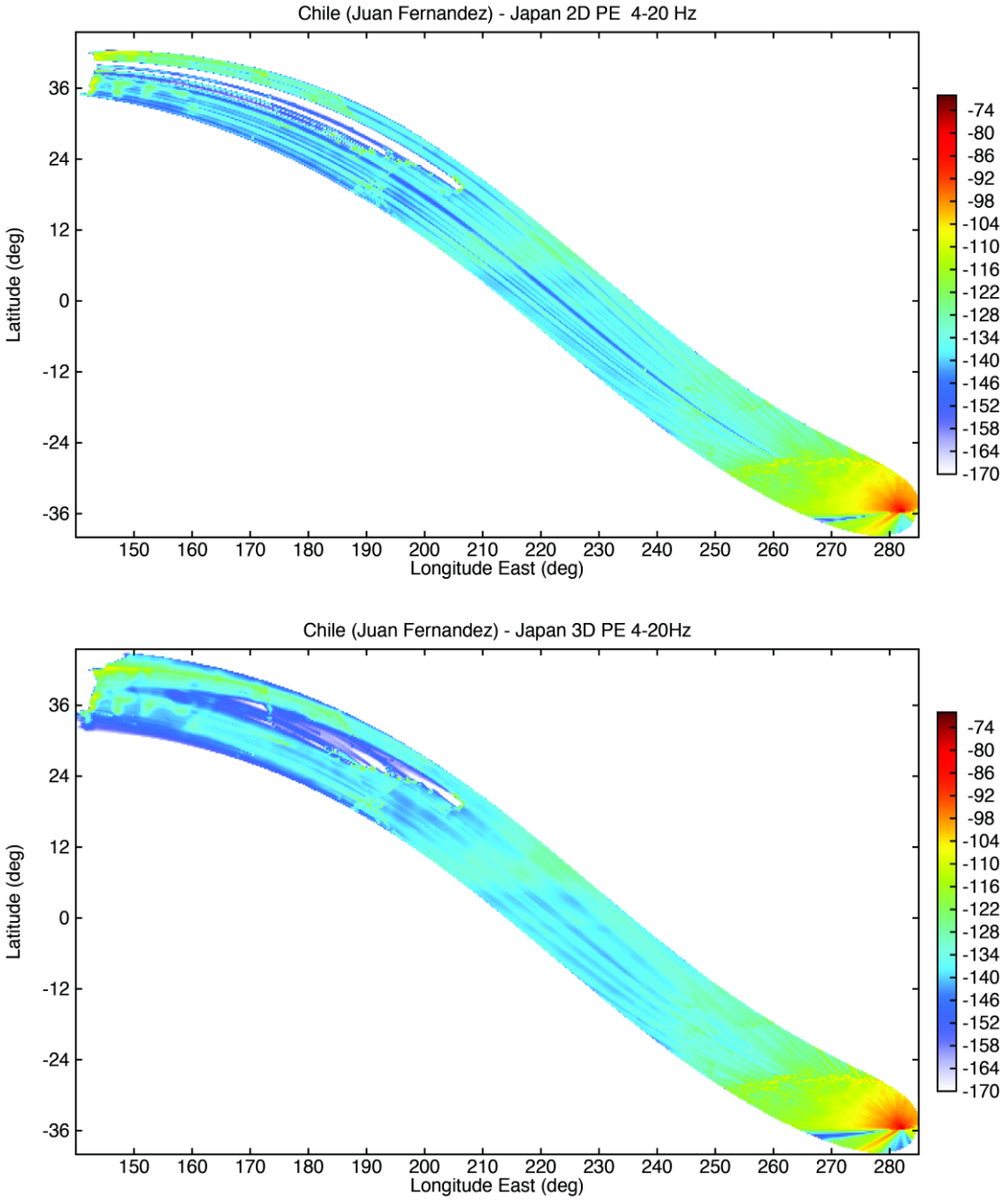

Figure 6. Broadband incoherent TL (4-20Hz) computed using the two-dimensional (top) and three-dimensional (bottom) Parabolic Equation (Peregrine) from Juan Fernandez (of Chile) to the Japanese Coast.

Dr. Heaney visited Professor Yamada and Dr's Mario Zampolli and Georgios Haralabus.at the UN Comprehensive Test Ban Treaty Organization in Vienna. The Yamada measurements, of large shots used as seismic sources off the coast of Japan received at the CTBTO HA03 station in Juan Fernandez Chile, are a treasure trove of long-range low frequency acoustic propagation. In conferring with the CTBTO scientists, it has become clear that acoustic out of plane scattering (forward reflections, refraction and diffraction) are significant observable effects. Dr. Heaney set up a broadband PE run in 3D to a range of 16700 km. Initially this was done for frequencies of 3-4 Hz for run-time considerations.

The technical results of the interactions are being collected into a Journal article. Some of the findings are summarized here. The move-out arrivals of the 100 shots on H03N1 are shown in Figure 7.

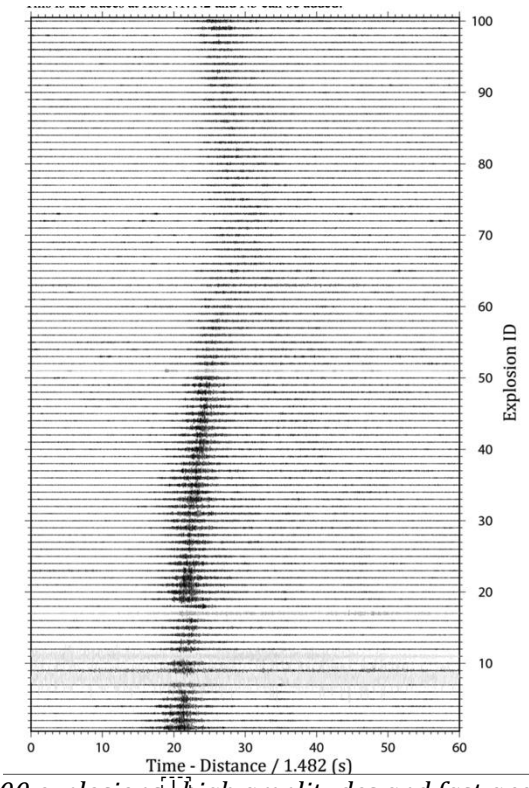

Figure 7. Signals from 100 explosions, high amplitudes and fast arrivals [1-50], low amplitude and slow arrivals [51-100]

A high energy arrival (20) is shown in Figure 8. Note the significant Signal-to-Noise ratio, the modal dispersion below 10Hz, the slight evidence of related arrivals at 38 and 48 s. The dominant frequency range of energy is clearly 10-40Hz. Unfortunately, this is higher than the band used for propagation modeling done in June. This will be addressed by pushing the PE model up in frequency during the month of July.

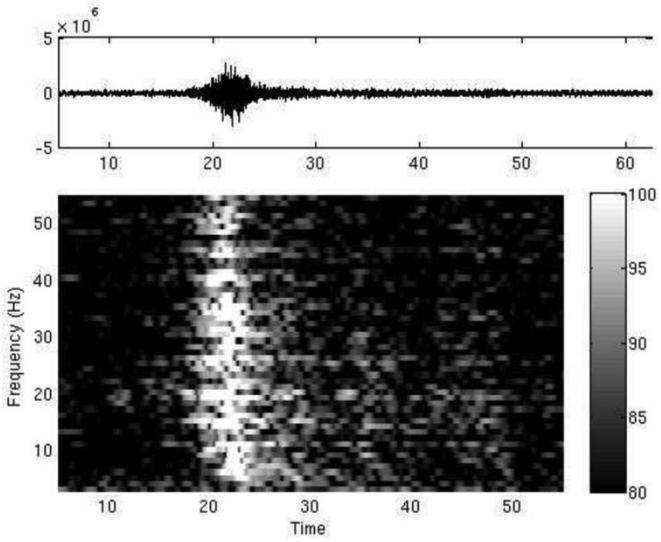

Figure 8. Time series (top) and spectrogram of shot 20.

The 3D PE was run, using reciprocity, from Juan Fernandez, Chile to each shot location off the coast of Japan. Peregrine has an option where the 3D code can be computed along a tube centered on the geodesic path. Initially this computational tube was set to 300km, as it was expected that the energy received in the shadow of Hawaii would refract around small islands and fill in the shadow. This turned out not to be the case. The energy observed in the shadow of the Hawaiian Islands is refracted from Midway, and thus the width of the computational tube must be set to 1000 km. The 4Hz run was performed and is compared with the observations in Figure 9.

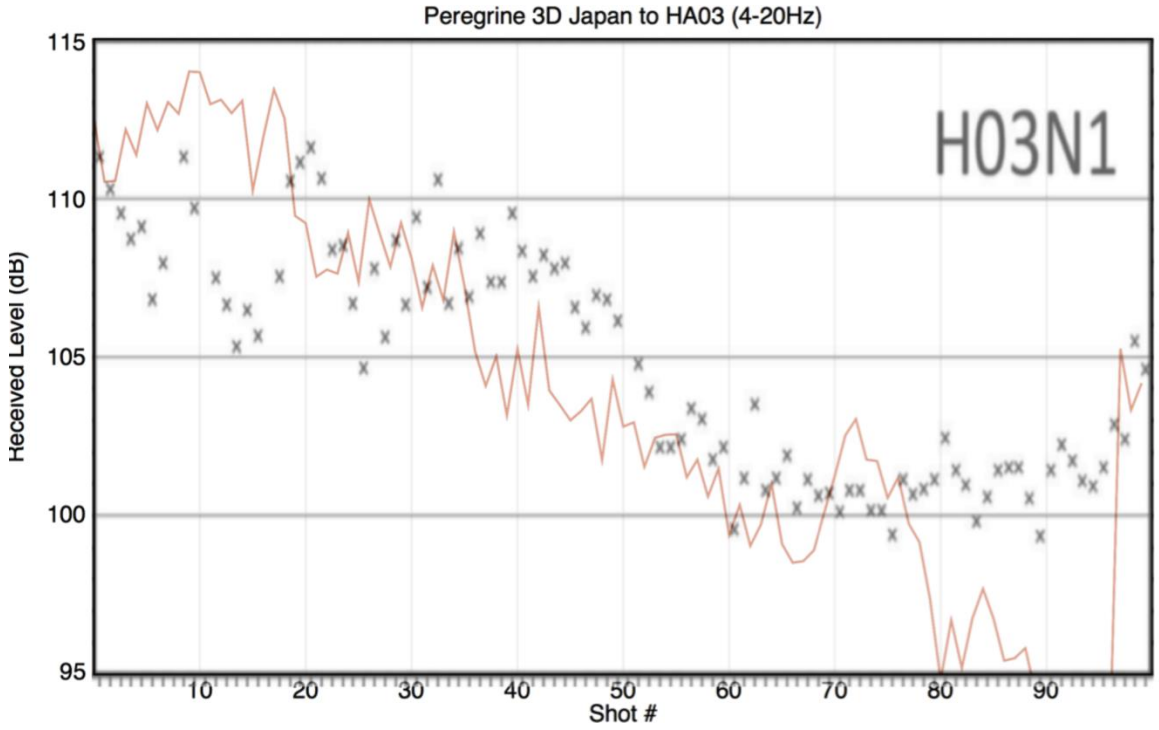

Figure 9. Received Sound Exposure Level (integrated energy over 5 s) for the data (*) and the 3D Peregrine Model (line) run at 4Hz.

The source level in this overlay is a free parameter (but is estimated to be ~215 dB) re $1uPa^2/m^2$). This agreement is exceptional. It shows the dip in received level by about 10 dB from shots 1-30 and shots 60-80. Note that the 2D computation has a dip of ~100 dB. The 3D computation with a 300 km computational tube had a dip of ~ 30 dB.

The broadband PE was run from 3-5Hz for each shot location. The ray-tube was set to 300 km, which is known to be deficient. Yet, the preliminary results are quite promising. The PE-data comparisons are shown in Figure 10, where the PE has been run for every 10^{th} shot.

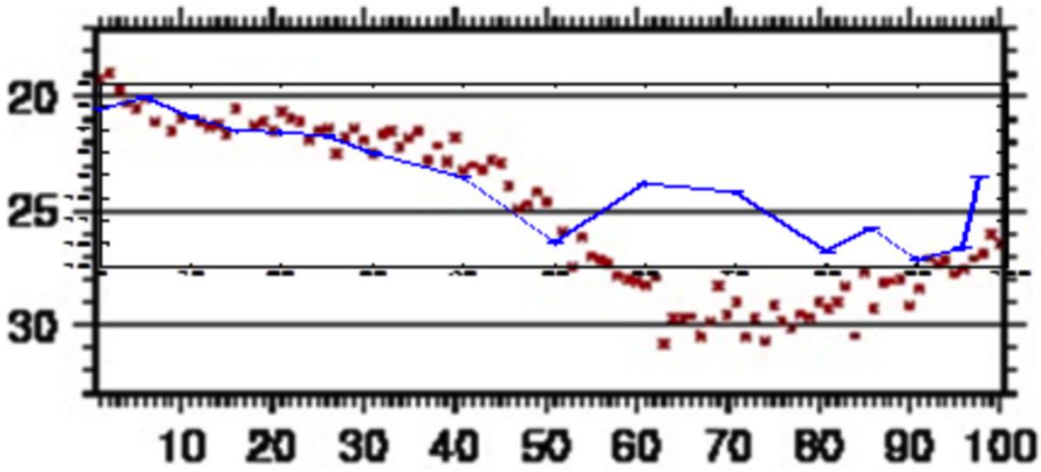

Figure 10. Arrival time (center of mass) of the measurements (*) and the model results (lines) for the 3D Peregrine Model (line) run from 3-5 Hz.

3.2. Passive Acoustic Thermometry

From theoretical considerations it follows that the acoustic travel time between two sensors can be obtained from the ambient noise field. In underwater acoustics, this travel time strongly depends on the depth and temperature and to a lesser extent on salinity (Dushaw et al. 2009). In order to apply this theory in long range ocean acoustics and derive deep ocean temperature, hydro-acoustic recordings from a station near Ascension Island are analyzed. This station, called H10, is in place for the verification of the Comprehensive Nuclear-Test-Ban Treaty and as such part of the International Monitoring System (IMS). H10 consists of two hydrophone triplets that are placed in the Sound Fixing and Ranging (SOFAR) channel (Dahlman et al. 2009). The SOFAR channel is a low-velocity layer in the deep ocean, i.e., the average channel axis depth is 1.5 km, which allows low frequency sound to be detected over long ranges (Munk & Forbes 1989). The efficiency of the SOFAR channel for sound propagation has already been used in studies related to earthquakes (Evers at al. 2004; De Groot-Hedlin 2005; Guilbert et al. 2005), icebergs (Chapp, Bohnenstiel & Tolstoy 2005; Talandier et al. 2006; Evers et al. 2013), explosions (Munk & Forbes 1989; Prior et al. 2011), marine mammals (Prior et al. 2012) and underwater volcanoes (Green at al. 2013). Guided wave propagation contributes to the limited acoustical attenuation by the SOFAR channel. In this study, the triplets are considered as arrays which are located to the north (7.84◦S, 14.49◦W) and south (8.95◦S,14.65◦W) of Ascension Island, at an inter-array distance of about 126 km, to avoid blocking by the island for sound coming from certain directions (see Figure 11).

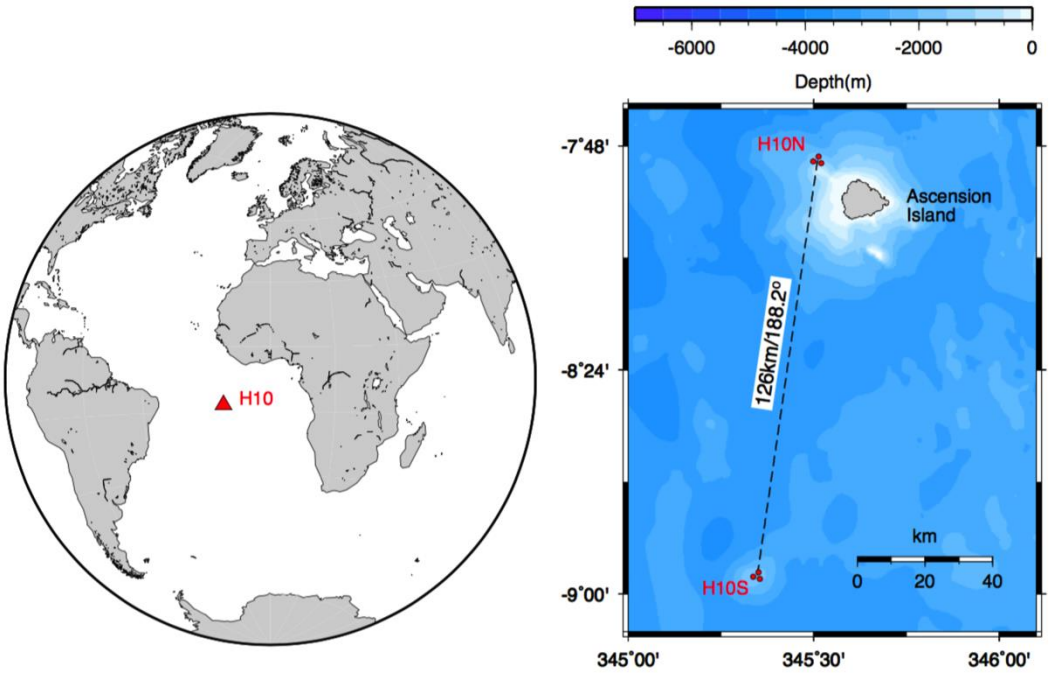

Figure 11. The location of H10 in the Atlantic Ocean near Ascension Island. H10 consists of two three-element hydrophone arrays, one to the north (H10N) and one to the south (H10S) of Ascension Island. The aperture of each array is about 2 km. The distance between the arrays is 126 km and the bearing connecting the two arrays is 188.2°.

Figure 12 shows the cross correlation results for a frequency of 0.5 to 15 Hz for 2011, May 5 between 11h and 12h UTC. The raw unfiltered recordings of N2 and S2 are also shown. It has been tested that this arbitrarily chosen day and hour are representative. The envelopes are calculated to accurately measure the peak of the cross correlation. It follows from Figure 12 that cross correlations for this day have coefficients up to 0.4. Significant cross correlation coefficients start to be retrieved from a frequency of 3 Hz and higher, which corresponds to the frequencies which the SOFAR channel can facilitate due to its limited thickness. Patches of energy in specific frequency bands appear more correlated than those in other frequency bands, which is typical for the modal propagation in the SOFAR channel (De Groot-Hedlin, Blackman & Jenkins 2009). As expected, the width of the envelope reduces with increasing frequency, enabling a higher time resolution. Furthermore, the lag time becomes smaller with increasing frequency. This can be understood by taking into account the shape of the SOFAR channel, where the lowest sound speed is at the channel axis. The smaller the wavenumber, the more the horizontal propagation energy is confined to the channel axis, which results in the larger lag times. As the frequency increases, more of the energy gets guided by the higher sound speeds surrounding the channel axis. In a ray-theoretical approach, the latter corresponds to rays being less horizontally incident on the receivers with increasing frequency. In this specific example, the difference in the lag time is 0.3 seconds, i.e., 85.5s at 4.3 Hz and 85.2s at 7.5 Hz.

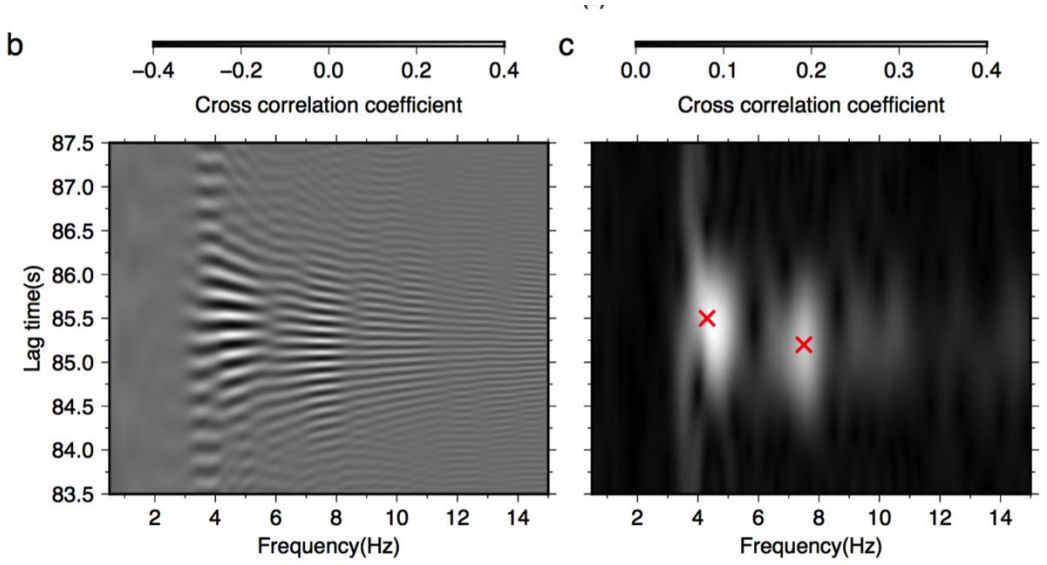

Figure 12. The cross correlation coefficients between N2 and S2 are shown for both (b) the cross correlation and (c) the envelop surrounding the cross correlation. These results are obtained with frequency bands of 1.0 Hz and a sliding window with steps of 0.1 Hz. The maxima (red crosses) are determined as 85.5s at 4.3 Hz and 85.2s at 7.5 Hz.

The Parabolic Equation Model (Peregrine) was used to model the impulse response (Green's Function) between the two receivers N2 and S2 for a 3-5Hz signal and a 5-10Hz signal. This propagation effort revealed that the ETOPO1 bathymetry model had significant difficulties (as the S2 receiver was actually deeper than the ETOPO reported bathymetry, which must be incorrect). The modeled arrival times do not quite match the observed 85.5 and 85.2 Hz, but the higher frequency model is 0.3 s faster than the lower frequency. Possibly there is an error in the range due to either the geodesic correction or the element positioning.

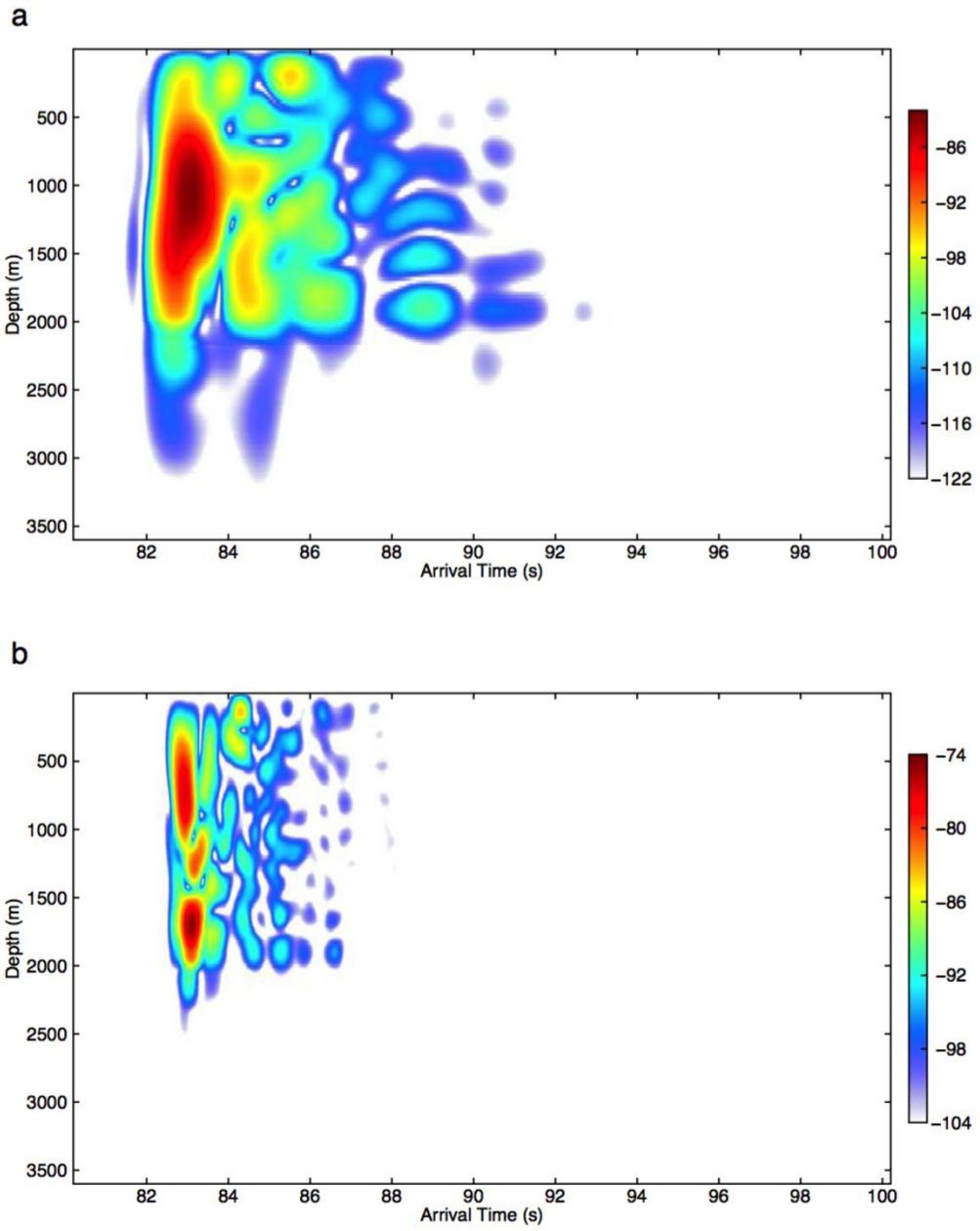

Figure 13. The travel time between N1 and S1 obtained from modeling with the parabolic equation. Results are shown for (a) the low frequency band of 3 to 5 Hz and (b) the high frequency band of 5 to 10 Hz.

3.3. Mesoscale Deflection of Basin Acoustic Transmission

Scenario

The scenario chosen to evaluate the impact of mesoscale variability on the arrival angle of long-range signals is a seismic event on the Kerguelen Plateau (-53°S 71°E) in the southern ocean. This region of the world, which includes Heard Island, Crozet Island and the Kerguelen Plateau has historical significance in the long-range

underwater community (Perth-Bermuda, HIFT) and is the position of the IMS hydro-acoustic station HA04. As demonstrated in the Heard Island Feasibility Test, sound sources here can be detected from the Southern Atlantic to the Pacific. The receiver position is taken be approximately at the IMS HA10S location (Ascension Island southern station). The hydroacoustic station at Ascension, as can be seen in Figure 14, has acoustic visibility to the South Atlantic, South Indian and South Pacific and has a large number of hydroacoustic signals generated by seismic events.

Results

Many of these results were reported in the previous July 15 Quarterly Progress Report. During this period of Performance the complete simulation time series was finished and the final back-azimuth versus year-day and frequency curve was generated.

The beamformer output was collapsed to a single back-azimuth value by computing the centroid of the beam power over the searched arrival angle. The time-series of the back-azimuth for the set of model simulations is shown Figure 14, along with the geodesic back-azimuth. There is substantially more deflection observed in the ECCO2 result than in the WOA09 result, indicating that the combined impact of the mesoscale eddies and sharper front definition is important to the acoustic propagation path. There is a long time-scale oscillation on the order of a 120-day period, ostensibly related to seasons, but it does not repeat for each season of 1992 to the corresponding season of 1993. This oscillation leads to the range in the back-azimuths going from a minimum near 141.5° to a maximum of 143.1°. The back-azimuth as a function of frequency does show coherent behavior, at least within the observed 0.3° small time scale variability. There is one outlier in the data. The July 28th, 1993 results exhibit a split arrival for 2, 4 and 8 Hz. This is evident faintly in Figure 14. This double arrival leads to a significant change to the centroid computation. There is a consistent 3-6 day oscillation in the back-bearing computation which could be due to small-scale motions of the eddies and the bathymetry. The monthly RMS of the arrival angle, which captures this oscillation, is 0.16°. There are no internal waves in the simulation.

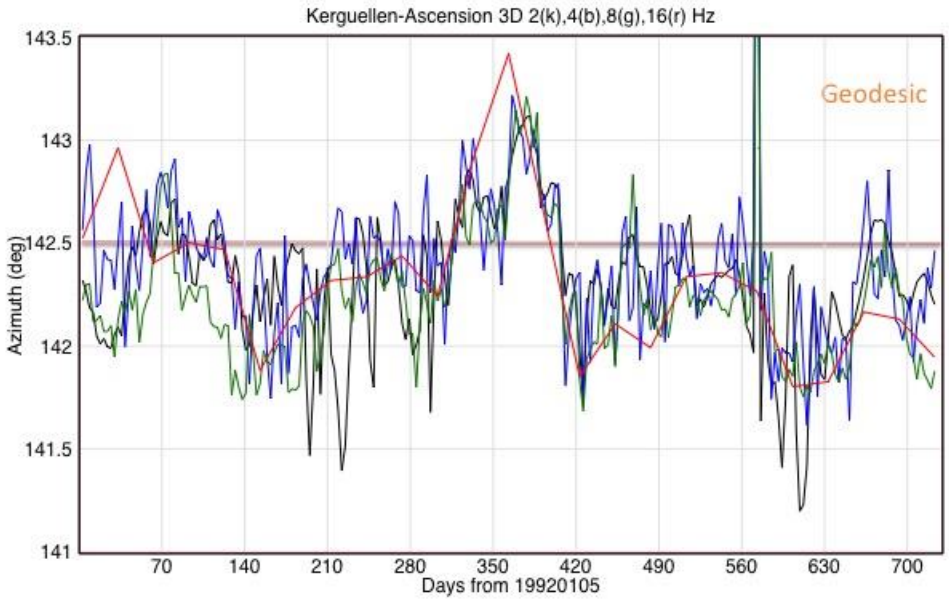

Figure 14. Centroid of arrival energy for 2-16 Hz over 1992-1993 Ecco2 model.

The deflection of basin-scale low-frequency acoustic propagation by mesoscale eddies and oceanic fronts was evaluated using a three-dimensional parabolic equation model. The 3D PE model Peregrine was introduced and applied to the simulated problem of the arrival of energy at the IMS station HA10S (Ascension) in the South Atlantic from an earthquake on the Kerguelen ridge in the south Indian Ocean. The field was computed for the World Ocean Atlas 2009 climatology and a two-year time series from the ECCO2 eddy-resolving re-analysis for the acoustic frequencies spanning 2 – 16 Hz. The back-azimuth was computed by beamforming on a roughly 13 km x 13 km two-dimension array centered near Ascension. The climatology ocean (WOA09) showed very little seasonal dependence or change from the geodesic and this is presumed to be due to the smoothing of the front due to the spatial and temporal averaging process of building the climatology. The ECCO2 results, on the other hand showed a deviation of back-azimuth ranging over a range of nearly 2° over the two year period. The back-azimuth was consistent across the frequency band and showed a 120-day "seasonal" oscillation.

The results presented here are consistent with the Munk's (Munk, 1980) prediction of an order of magnitude of 1° deflection. They are larger than the observations made by Voronovich *et.al.(Voronovich et al., 2005) (*RMS ~ 0.36°) and numerical results of Dushaw(Dushaw, 2014) (~0.2°), which can be explained by the larger

propagation distance and the more dynamic Agulhas retroflection region compared to the North Eastern Pacific.

Dushaw's conclusion was that horizontal refraction has a negligible impact on ocean acoustic tomography and regional submarine source localization. For global scale seismic or nuclear event detection, however, this effect can be significant. The implications of a 1° error in back-azimuth for localization are significant for propagation at basin scale ranges (9100 km for this case). A simpler $\Delta\theta$ calculation for a bearing error of 1° yields a position offset of 158 km for this example. The impact of this is illustrated in Figure 15 where the geodesic connecting the source / receiver and the back-azimuth line are plotted overlaid on the 3D depth averaged Transmission Loss result.

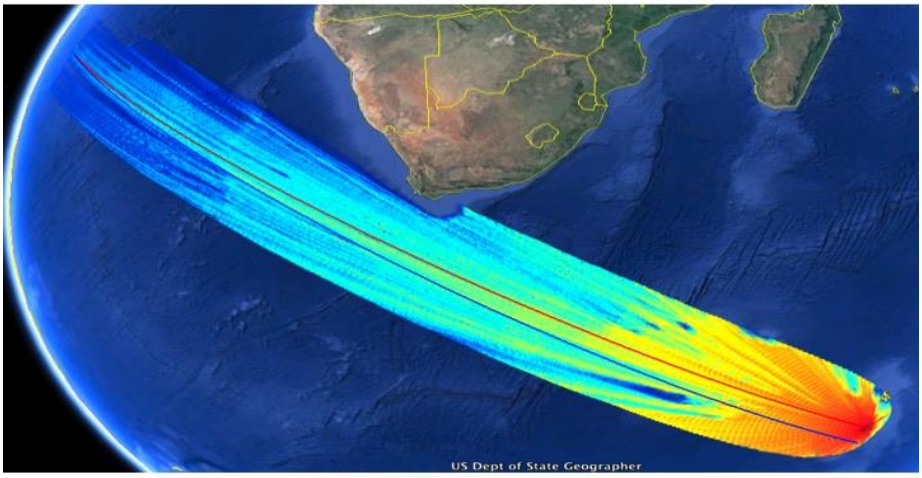

Figure 15. Localization error (southern line) using back-azimuth compared with source-receiver geodesic (northern line) overlaid on the 4Hz 3-dimensional acoustic field (color online)

4. NPAL PhilSeal0 Data Analysis and Matched Field Processing

During the Philippine Sea 2010 experiment, Dr. Peter Worcester (SIO) deployed a large full-water column spanning vertical line array and Dr. Heaney and Prof. Baggeroer (MIT) deployed a source to transmit waveforms to the array. One of the more interesting results to date is the evidence of strong narrowband interference patterns in the data with depth as the source was towed within 1-CZ of the array. These are shown in Figure 16.

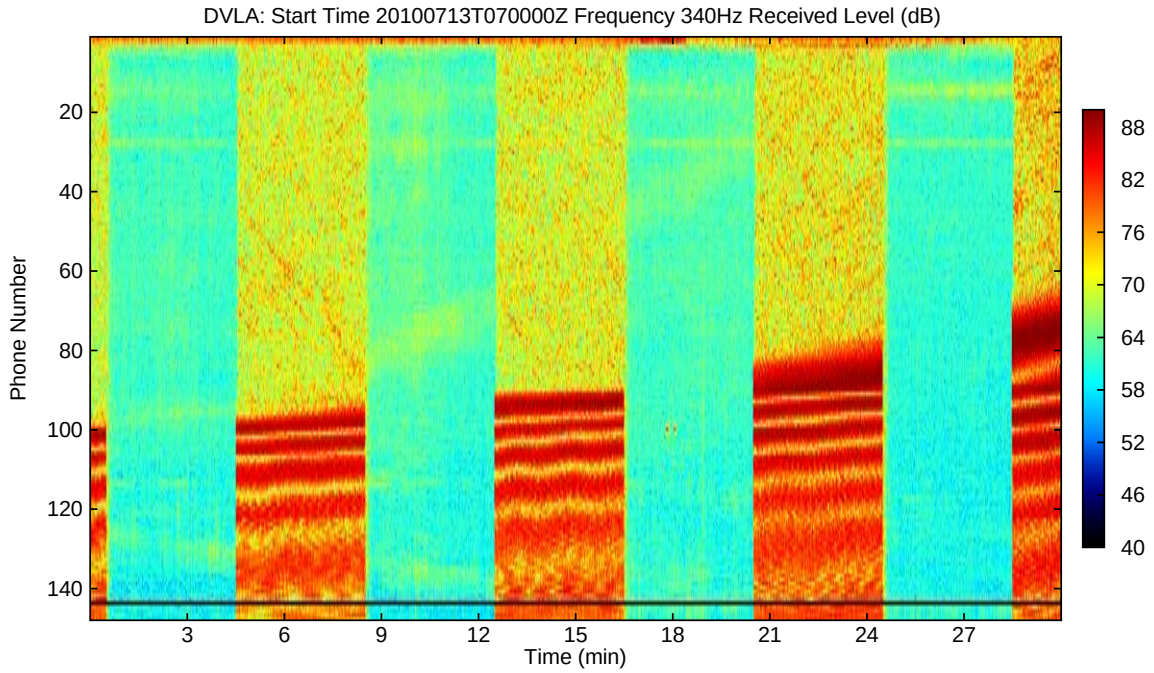

Figure 16. Narrowband (340Hz) received level vs. Phone Number (similar to depth) as function of time as the source moved from 10-20 km away.

The structure of this interference pattern is significant, even if it should not be surprising. This is the Lloyd's mirror pattern from the coherent surface reflection, after it has refracted from near the surface to depth. The presence and behavior of these interference patterns are completely predictable (up to moderate sea-states) and can be used as a target classification (submerged/surface) and ranging tool, even for single deep hydrophone receivers, such as the NOGAPS system. Dr. Heaney and his team will be investigating the possibilities of autonomous classification and ranging in the near future.

4.1. NPAL PhilSeal0 Ambient Noise Analysis and Modeling

PhilSea09 analysis involved noise modeling and analysis of the vertical directivity from the PS09 Vertical Line Array. PS09 was chosen because this VLA was spaced at $\lambda/2$ at 250Hz and is therefore beamforming capable, covering the conjugate depth.

An ambient noise model was built for predicting the vertical noise component of the ambient noise. The model used Peregrine for hydrophone to $\lambda/4$ depth below the surface (for a noise sheet and for ships) to the edge of the Philippine Sea basin. Wind speed was computed by adding each surface patch to the array cross-spectral density (corresponding to the Kuperman-Ingenito surface sheet of independent sources). Shipping was input via a realization of the HITS model for the Philippine Sea. The results are dependent upon the seafloor. For a soft sediment, the modeled

vertical noise directivity at the axis and at the conjugate depth are shown in Figure 17.

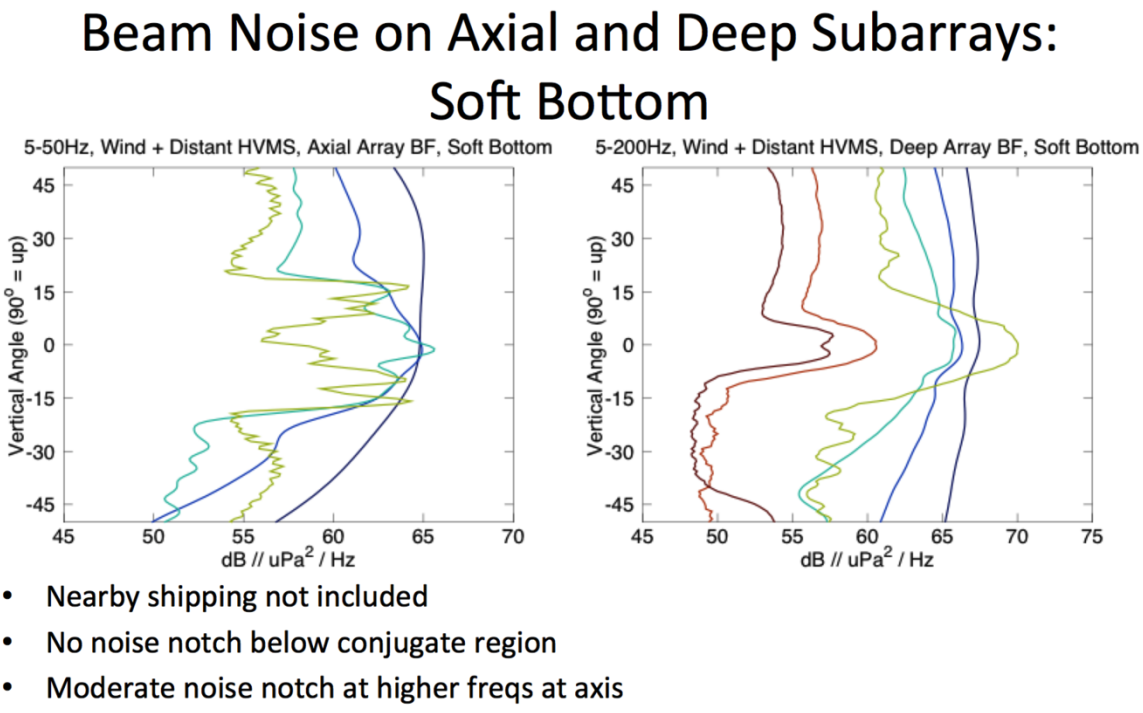

Figure 17. Vertical Noise Directivity as a function of frequency for an axial (left) and deep (right) vertical line array for frequencies from 5-50Hz (axial array) and 5-200Hz. – Which are the unaliased beamforming capable frequencies of the deployed arrays.

We now compare the deep VLA noise vertical directivity of the measurement from those modeled using a hard seafloor and a soft seafloor. The result is shown in Figure 18, indicating the seafloor is best modeled as hard.

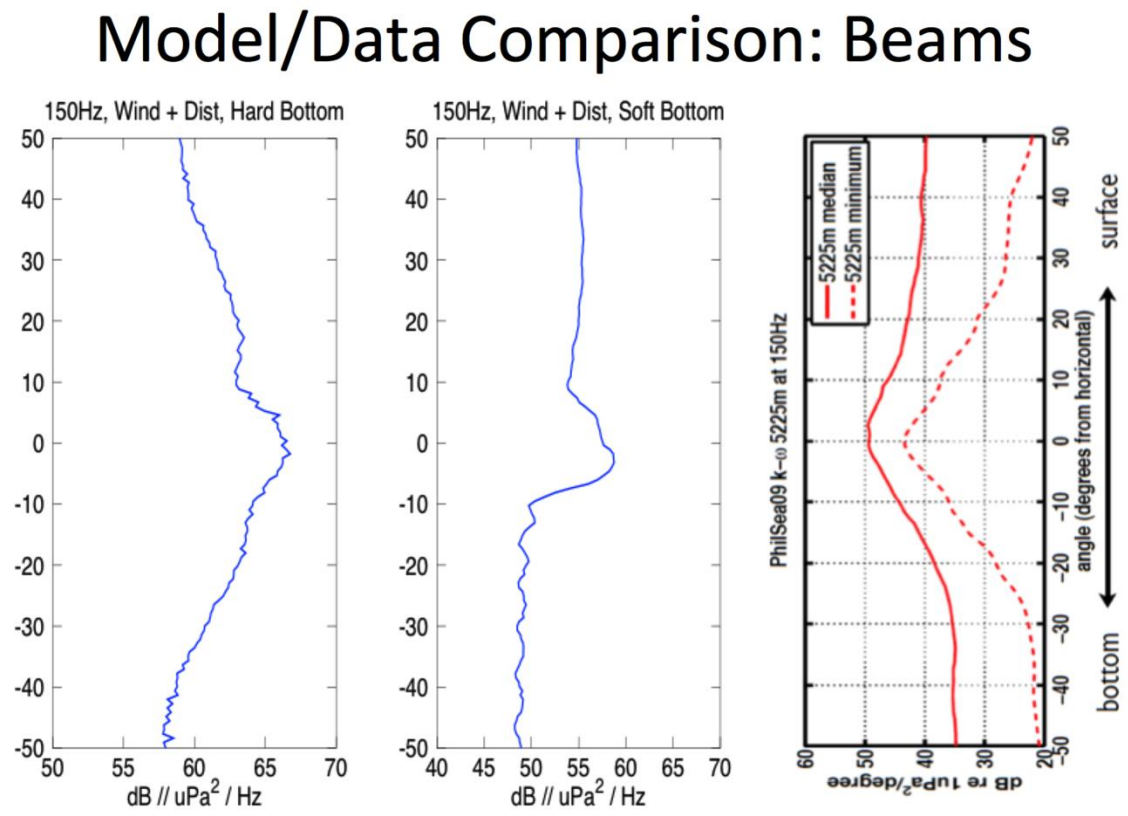

Figure 18. Vertical Noise Directivity for 150Hz using a hard seafloor (left), soft (middle) and from the observations. The lack of a clear critical angle indicates a harder sediment.

The deep VLA data was processed for 24 hours. The band averaged, Hann-windowed BTR (Bearing Time Record) of vertical angle vs. time is shown in Figure 19.

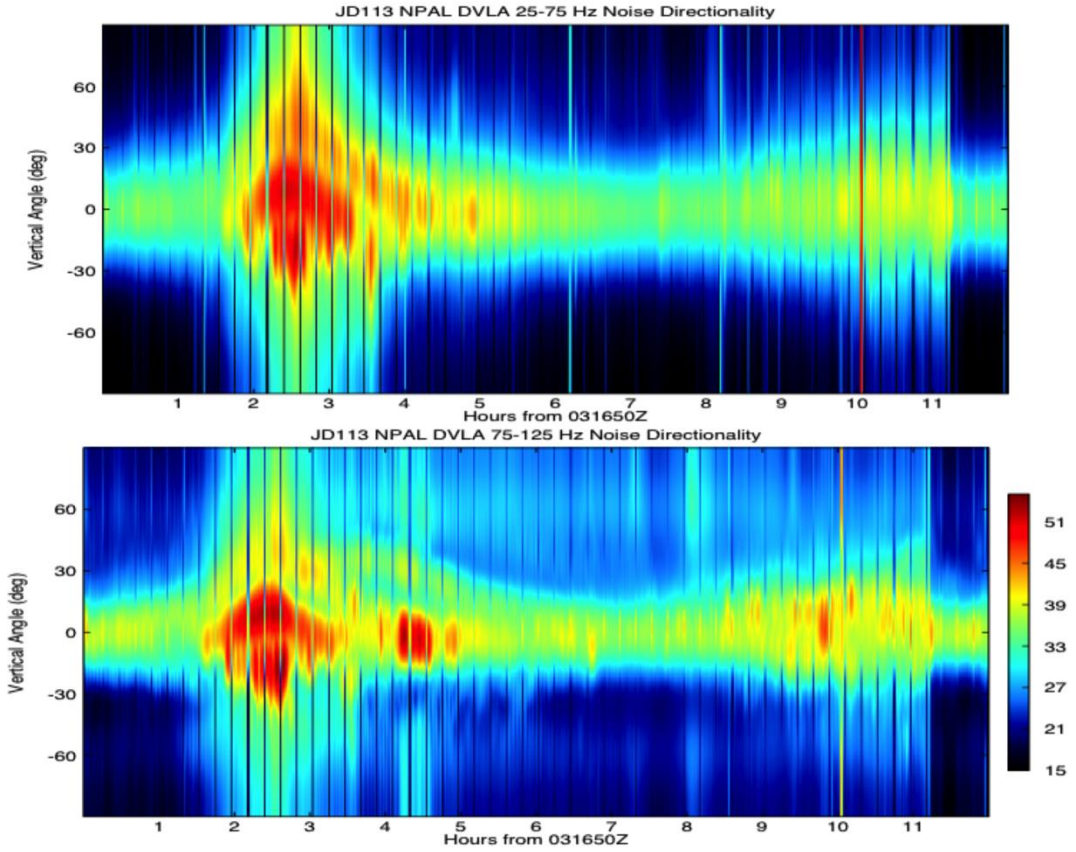

Figure 19. Bearing Time Records for 25-75 Hz and 75-125Hz for the DVLA on Julian Day 113. The CPA of the R/V Revelle is seen at hour 2:30.

The CPA of the surface ship is evident at hour 2, with the associated high angle energy, particularly at low frequency. Note the energy, particularly in the upper band during the quiet periods that is coming in from the above the array (positive vertical angles). This is wind energy from above. It is not evidently coming from below, a physical phenomenon Harrison attributed to the bottom energy having 1 more bottom bounce. This leads to the technique of estimating the reflection coefficient by subtracting the downward energy from the upward energy (for each corresponding beam). The result of this operation is the estimated reflection coefficient vs. frequency and is shown in Figure 20.

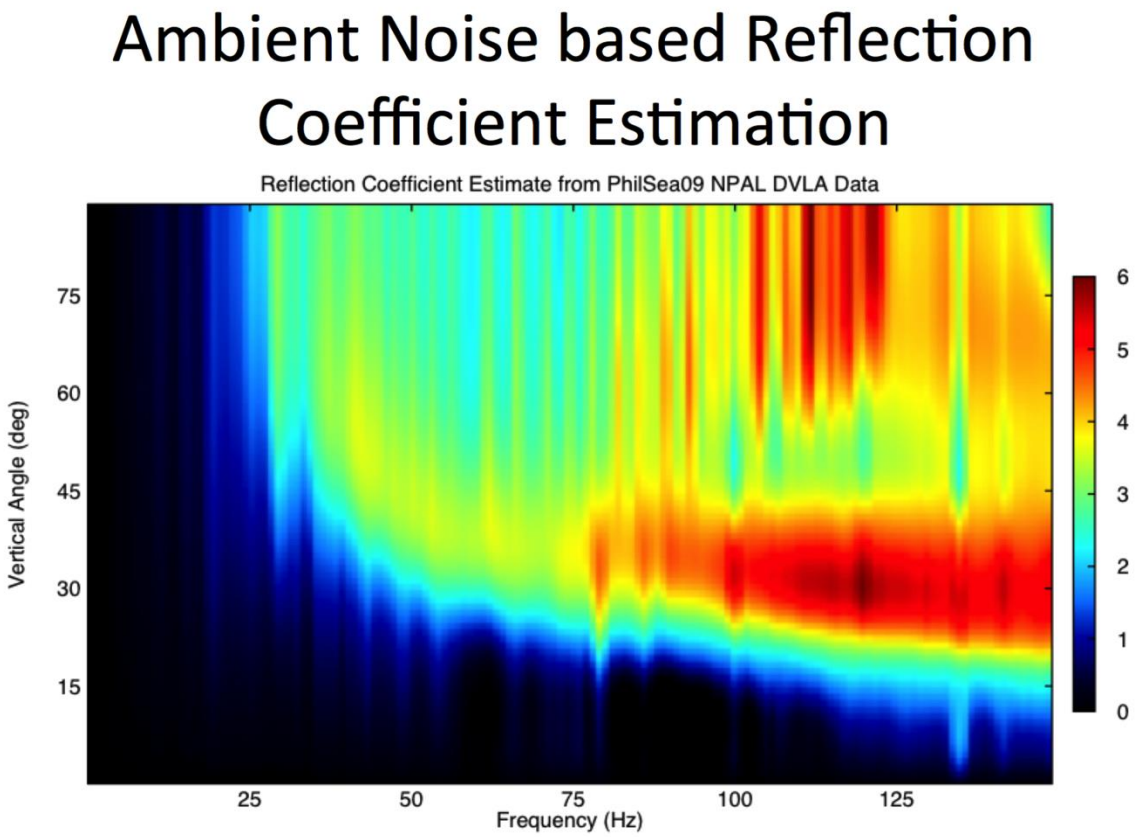

Figure 20. Estimated reflection coefficient as a function of frequency by taking the difference of downgoing and upgoing energy.

5. Publications and Peer Interactions

Dr. Heaney submitted a paper, as a co-author with Dr. Laslo Evers of KNMI (The Dutch Meteorological Institute) to the Geophysical Journal International entitled: *"Deep ocean sound speed characteristics passively derived from the ambient acoustic noise field".*

Revisions where made to "Bathymetric diffraction of basin-scale hydroacoustic signals" by Kevin D. Heaney, Richard L. Campbell and Mark Prior, and it was re-submitted to Journal of the Acoustical Society of America on August 30, 2016.

Dr. Heaney presented at the CTBTO Infrasound workshop, Vienna October 2015, a paper and discussed issues associated with the test ban treaty verification with Dr. Georgios Haralabus and Dr. Mario Zampolli, as well as infrasound modeling with researchers at KNMI (The Royal Dutch Meteorological Institute).

Evers, L. G., Brown, D. J., Heaney, K. D., Assink, J. D., Smets, P. S. M., and Snellen, M. (**2014**). "Evanescent wave coupling in a geophysical system: Airborne acoustic signals from the Mw 8.1 Macquarie Ridge earthquake," Geophysical Research Letters **40**.

Haney, M. M., Chadwick, B., Merle, S., Buck, N. J., Butterfield, D., Coombs, M., Heaney, K. D., Lyons, J., Searcy, C., Walker, S., Young, C., and Embley, R. (**2014**). "The 2014 submarine eruption of Ahyi Volcano, Northern Mariana Islands," in *AGU General Meeting 2014*, edited by A. G. Union (San Francisco).

Heaney, K. D., and Campbell, R. L. (**2015**). "Parabolic Equation Modelling of Acoustic Propagation on Small Moons," in *International Congress on Sound and Vibration* (International Institute of Acoustics and Vibration, Florence).

Heaney, K. D., and Campbell, R. L. (**2016**). "Three-dimensional parabolic equation modeling of mesoscale eddy deflection," Journal of the Acoustical Society of America **139**, 918-926.

Miksis-Olds, J., Vernon, J. A., and Heaney, K. D. (**2014a**). "Applying the dynamic soundscape to estimates of signal detection," in *Underwater Acoustics Conference* (Rhodes, Greece).

Miksis-Olds, J., Vernon, J. A., and Heaney, K. D. (**2014b**). "Global ocean sound behavior and its impact on translating soundscapes into acoustic communication range for signal detection," in *5th Intergovernmental Conference on the Effects of Sounds in the Ocean on Marine Mammals* (Amsterdam).

6. References

Brown, M. G., Godin, O. A., Williams, N. J., Zabotin, N. A., Zabotina, L., & Banker, G. J., 2014. Acoustic Green's function extraction from ambient noise in a coastal ocean environment, *Geophys. Res. Lett.*, 41, 5555–5562.

Chapp, E., Bohnenstiel, D. R., & Tolstoy, M., 2005. Sound-channel observations of ice-generated tremor in the Indian Ocean, *Geochemistry Geophysics Geosystems*, 6, Q06003.

Chen, X. & Tung, K. K., 2014. Varying planetary heat sink led to global-warming slowdown and acceleration, *Science*, 345, 897–903.

Collins, M. D., 1993. A split-step Pade´ solution for the parabolic equation method, *J. Acoust. Soc. Am.*, 93, 1736–1742.

Dahlman, O., Mykkeltveit, S., & Haak, H., 2009. *Nuclear Test Ban*, Springer.

De Groot-Hedlin, C., Blackman, D. K., & Jenkins, C. S., 2009. Effects of variability associated with the Antarctic circumpolar current on sound propagation in the ocean, *Geophys. J. Int.*, 176, 478–490.

De Groot-Hedlin, C. D., 2005. Estimation of the rupture length and velocity of the Great Sumatra earthquake of Dec 26, 2004 using hydroacoustic signals, *Geophys. Res. Lett.*, 32, L11303.

Dushaw, B. D., Worcester, P. F., Munk, W. H., Spindel, R. C., Mercer, J. A., Howe, B. M., Metzger, K., Birdsall, T. G., Andrew, R. K., Dzieciuch, M. A., Cornuelle, B. D., & Menemenlis, D., 2009. A decade of acoustic thermometry in the North Pacific Ocean, *J. Geophys. Res.*, 114, C07021.

Evers, L. G. & Snellen, M., 2015. Passive probing of the sound fixing and ranging channel with hydro-acoustic observations from ridge earthquakes, *J. Acoust. Soc. Am.*, 137, 2124–2136.

Evers, L. G., Green, D. N., Young, N. W., & Snellen, M., 2013. Remote hydroacoustic sensing of large icebergs in the southern Indian Ocean: Implications for iceberg monitoring, *Geophys. Res. Lett.*, 40, 4694–4699.

Evers, L. G., Brown, D., Heaney, K. D., Assink, J. D., , Smets, P. S. M., & Snellen, M., 2014. Evanescent wave coupling in a geophysical system: Airborne acoustic signals from the mw 8.1 Macquarie Ridge earthquake, *Geophys. Res. Lett.*, 41, 1644–1650.

Green, D. N., Evers, L. G., Fee, D., Matoza, R. S., Snellen, M., Smets, P., & Simons, D., 2013. Hydroacoustic, infrasonic and seismic monitoring of the submarine eruptive activity and sub-aerial plume generation at South Sarigan, May 2010, *J. Volc. and Geothermal Res.*, 257, 31–43.

Guilbert, J., Vergoz, J., Schissele´, E., Roueff, A., & Cansi, Y., 2005. Use of hydroacoustic and seismic arrays to observe rupture propagation and source extent of the Mw = 9.0 Sumatra earthquake, *Geophys. Res. Lett.*, 32, L15310.

Dushaw, B. D. (2014). "Assessing the horizontal refraction of ocean acoustic tomography signals using high-resolution ocean state estimates," *The Journal of the Acoustical Society of America 136, 122-129.*

Munk, W. (1980). "Horizontal deflection of acoustic paths by mesoscale eddies," *Journal of Physical Oceanography 10, 596-604.*

Voronovich, A. G., Ostashev, V. E., Group, T. N., Colosi, J. A., Cornuelle, B. D., Dushaw, B. D., Dzieciuch, M. A., Howe, B. M., Mercer, J. A., Munk, W., Spindel, R., and Worcester, P. F. (2005). "Horizontal Refraction of acoustic signals retrieved from North Pacific Acoustic Laboratory billboard array data," *Journal of the Acoustical Society of America 117, 1527-1537.*

7. Financial Summary

OASIS, INC.
JOB STATUS REPORT **12/31/2016**

1172 DEEP WATER ACOUSTICS **N00014-114-C-0172**
POP: 9/27/13-12/30/16

CONTRACT VALUE	Cost	Fee	Total
Contract Value	$368,935	$27,048	$395,983
Funding Value:	**$368,935**	**$27,048**	**$395,983**
Remaining to Fund:	$0	$0	$0

CUMULATIVE SPENDING WITH COMMITMENTS

	DIRECT	OH	MH	TOTL COST	FEE	**TOTAL**
ACTUAL						
OASIS	$207,929	$155,328	$4,487.13	$367,744	$27,581	**$395,325**
COMMITTED						
	$0	$0	$0	$0	$0	**$0**
	$207,929	$155,328	$4,487	$367,744	$27,581	**$395,325**
TOTAL REMAINING TO SPEND:						**$658**